Mammogram Image Superresolution Based on Statistical Moment Analysis

Alexander Wong, Akshaya Mishra, David A. Clausi, and Paul Fieguth
Vision and Image Processing (VIP) Research Group
Department of Systems Design Engineering
University of Waterloo, Waterloo, Canada
{a28wong,akmishra,dclausi,pfieguth}@uwaterloo.ca

Abstract

A novel superresolution method for enhancing the resolution of mammogram images based on statistical moment analysis (SMA) has been designed and implemented. The proposed SMA method enables high resolution mammogram images to be produced at lower levels of radiation exposure to the patient. The SMA method takes advantage of the statistical characteristics of the underlying breast tissues being imaged to produce high resolution mammogram images with enhanced fine tissue details such that the presence of masses and microcalcifications can be more easily identified. In the SMA method, the superresolution problem is formulated as a constrained optimization problem using an adaptive third-order Markov prior model, and solved efficiently using a conjugate gradient approach. The priors are adapted based on the inter-pixel likelihoods of the first moment about zero (mean), second central moment (variance), and third and fourth standardized moments (skewness and kurtosis) from the low resolution images. Experimental results demonstrate the effectiveness of the SMA method at enhancing fine tissue details when compared to existing resolution enhancement methods.

1 Introduction

According to the World Health Organization International Agency for Research on Cancer, breast cancer is the most frequent form of cancer in women worldwide, with an estimated 636,000 incidents in developed countries and 514,000 incidents in developing countries during 2002 [1]. Furthermore, breast cancer is also the leading cause of cancer-related deaths in women in many countries, with an estimated 519,000 deaths worldwide in 2004 [2]. Finally, according to the American Cancer Society, women with breast cancer have an increased risk of developing a second primary cancer [3]. One of the most effective approaches to reducing the risk of death due to breast cancer is early breast examination and screening of asymptomatic women. The most widely used technology for breast examination is mammography, where X-ray images of the breasts are acquired and analyzed to identify possible signs of abnormality such as the masses and microcalcifications. By detecting preclinical cancer before it is palpable and causes symptoms, breast cancer can be treated at an early stage to significantly improve survival rate as well as reduced complications associated with intensive treatment required for late-stage breast cancer [4].

Despite the effectiveness of mammography in early breast cancer detection, asymptomatic women are often hesitate to perform the procedure due to the potential harm caused by mammography. Besides patient anxiety and discomfort, the main cause of potential harm during the mammography procedure is patient exposure to harmful ionizing radiation. Therefore, minimizing patient exposure to harmful ionizing radiation is important to reduce the potential harm caused by mammography. However, a reduction in radiation dosage can result in a decrease of signal-to-noise ratio (SNR), which reduces image quality and affects the visibility of suspicious cancer-related abnormalities such as masses and microcalcifications. While SNR can be significantly improved at lower radiation dosages through the use of larger detector pixel dimensions, this comes at the expense of image resolution.

A technological solution showing great potential for achieving high SNR at lower radiation dosages without compromising image resolution is multi-source superresolution, where multiple low radiation images are combined to form a high-resolution image. In the multi-source superresolution approach proposed by Robinson et al. [5], a series of spatially shifted low radiation images were acquired of the object of interest, and combined into a high resolution image based on their relative alignments. In operational situations, these spatial shifts can be achieved through X-ray tube rotations, moving the object of interest with respect to the X-ray source, or using sensor arrays that are spatially shifted by a known displacement [6]. Robinson et al. [5]

978-0-7695-4040-5/10 $26.00 © 2010 IEEE
DOI 10.1109/CRV.2010.51

showed that mammogram images with similar image quality as a single image acquired at a normal radiation dosage of 226 mAs, can be produced by combining multiple low radiation images at a significantly reduced combined dosage of 169.5 mAs. Hence, superresolution techniques allows for the construction of mammogram images with higher image quality than can be achieved by the physical radiographic hardware in a single image at a given dosage, thus reducing potential harm to the patient while enhancing the visibility of suspicious cancer-related abnormalities for clinical diagnosis.

Given the benefits of multi-source image superresolution, several methods have been proposed for the purpose of enhancing medical images. Peeters et al. [7] proposed to employ a maximum a posteriori (MAP) estimation approach to combine functional magnetic resonance imaging (fMRI) data to produce high resolution data with reduced slice thickness, where the posterior probability distribution of the superresolution problem is maximized. Robinson et al. [5] also employed a MAP estimation approach to combine spatially-shifted low radiation X-ray images into a high resolution X-ray image. Peled and Yeshurun [8], Greenspan et al. [9], and Kennedy et al. [10, 11] utilized a variant of the iterative back-projection (IBP) method proposed by Irani et al. [12] to construct high resolution diffusion tensor magnetic resonance (DTMR), fast-spin echo (FSE) MR, and positron emission tomography (PET) images, respectively, from spatially-shifted images, where the high resolution image estimate is refined based on the error between its derived low resolution images and the actual low resolution images. Hsu et al. [13] proposed to construct high resolution cardiovascular images from low resolution imagery using a Projection on Convex Sets (POCS) [14] approach, where a high-resolution image estimate is projected onto each constraint within the convex constraint set until the desired condition is satisfied.

The main limitation of these multi-source superresolution approaches for enhancing mammogram images is that they do not take into account the underlying tissue characteristics of the breast region being imaged in the high resolution image construction process. As such, an alternative approach to multi-source superresolution that takes advantage of the underlying tissue characteristics can potentially yield great benefits for enhancing the visibility of suspicious tissue anomalies such as masses and microcalcifications, which is critical for early clinicial diagnosis of breast cancer.

The main contribution of this paper is SMA, a novel superresolution method for constructing high resolution mammogram images from a set of low resolution mammogram images. The high resolution image is adaptively generated for improved visibility of tissue detail based on the underlying tissue statistical characteristics of the low resolution images. The mammogram image superresolution problem is formulated in Section 2. The proposed SMA method is described in Section 3. Experimental results are presented and discussed in Section 4. Finally, conclusions are drawn in Section 5.

2 Problem Formulation

It is important to first define and formulate the mammogram image superresolution problem. Suppose that a set of n spatially shifted low resolution mammogram images $f_1, f_2, ..., f_n$ of size $M \times N$ were acquired of the same breast region using a dedicated mammography machine. From a theoretical perspective, each low resolution mammogram image can be alternatively viewed as a single high resolution mammogram image g of size $RM \times RN$ that has been spatially shifted, degraded (e.g., blurred), and downsampled by a factor of R. Given that each low resolution mammogram image is subject to different shifts and degradations, a particular low resolution mammogram image f_i can be represented in matrix-vector form as

$$\left(\underline{f}_i\right)_{:} = \mathrm{H_i} \left(\underline{g}\right)_{:} + \underline{n}_i, \tag{1}$$

where, $\left(\underline{f}_i\right)_{:}$ is an $[MN \times 1]$ vector representing a low resolution mammogram image f_i in lexicographic ordering, $\left(\underline{g}\right)_{:}$ is an $[R^2MN \times 1]$ vector representing the high resolution mammogram image g in lexicographic ordering, $\mathrm{H_i}$ is an $[MN \times R^2MN]$ matrix representing the observation model for a low resolution mammogram image, and $\underline{n}_i$ is an $[MN \times 1]$ vector representing noise in a low resolution mammogram image in lexicographic ordering. The observation model H consists of multiple degradations (e.g., spatial shift and blur) and can be formulated based on the intrinsic properties of the dedicated mammographic device.

Given Eq. (1), the relationship between the high resolution mammogram image g and the set of n spatially shifted low resolution mammogram images $f_1, f_2, ..., f_n$ can be formulated as

$$\begin{bmatrix} \left(\underline{f}_1\right)_{:} \\ \left(\underline{f}_2\right)_{:} \\ \vdots \\ \left(\underline{f}_n\right)_{:} \end{bmatrix} = \begin{bmatrix} \mathrm{H_1} \\ \mathrm{H_2} \\ \vdots \\ \mathrm{H_n} \end{bmatrix} \left(\underline{g}\right)_{:} + \begin{bmatrix} \underline{n}_1 \\ \underline{n}_2 \\ \vdots \\ \underline{n}_n \end{bmatrix}. \tag{2}$$

Alternatively, Eq. (2) can be expressed in a simplified form,

$$\overline{\underline{f}} = \overline{\mathrm{H}} \left(\underline{g}\right)_{:} + \overline{\underline{n}}, \tag{3}$$

where $\overline{\underline{f}}$ is a vector of stacked low resolution mammogram image vectors $\underline{f}_1, \underline{f}_2, ..., \underline{f}_n$, and $\overline{\mathrm{H}}$ is a matrix of stacked

observation matrices $\mathrm{H}_1, \mathrm{H}_2, ..., \mathrm{H}_n$. Given Eq. (3), the mammogram image superresolution problem is essentially an inverse problem, where the high resolution mammogram image g is estimated based on the observation models H and the low resolution mammogram images $f_1, f_2, ..., f_n$. In practice, only a few acquisitions can be made to limit potential harm to the patient. Therefore, only partial information about the high resolution mammogram images is gained from the low resolution mammogram images. Hence, the mammogram image superresolution problem is underdetermined and there are no unique solutions.

3 Proposed SMA Mammogram Image Superresolution Method

The proposed SMA mammogram image superresolution method can be summarized as follows. First, local tissue distributions in the low resolution mammogram images are modeled using sets of statistical moments. Second, the mammogram image superresolution problem is formulated as a constrained optimization problem using third-order Markov prior constraints that are adapted on a per-pixel level based on the inter-pixel likelihoods between the local tissue distributions. This constrained optimization problem is then solved efficiently using a conjugate gradient approach.

3.1 Local Tissue Distribution Modeling using Statistical Moments

The underlying goal of the SMA method is to construct high resolution mammogram images that better capture fine tissue details such that the visibility of suspicious cancer-related abnormalities such as masses and microcalcifications is improved. Therefore, intuitively, the SMA method should take into account the underlying tissue characteristics of the breast region captured in the low resolution mammogram images. As an initial step towards this goal, we propose to first model the local tissue distributions in the low resolution mammogram images. The motivation behind modeling the local tissue distributions is that pixels in the low resolution mammogram images with similar local tissue distributions are more likely to have similar tissue characteristics. Therefore, by taking advantage of pixels with similar tissue characteristics during the superresolution process, fine tissue details can be better preserved in the resulting high resolution mammogram image.

To capture the local tissue characteristics of the low resolution mammogram images, we propose to model the local tissue distribution Υ of each pixel $\underline{x} = (x, y)$ from a low resolution mammogram image using the first moment about zero m_1,

$$m_1(\underline{x}) = E\left[f(\underline{X})\right] = \frac{1}{Z_{\mathbb{N}}} \sum_{\underline{x} \in \mathbb{N}} f(\underline{x}_i), \tag{4}$$

the second central moment m_2,

$$m_2(\underline{x}) = E\left[(f(\underline{X}) - E[f(\underline{X})])^2\right] = \frac{1}{Z_{\mathbb{N}}} \sum_{\underline{x} \in \mathbb{N}} \left[f(\underline{x}_i) - m_1(\underline{x})\right]^2, \tag{5}$$

the third standardized moment m_3,

$$m_3(\underline{x}) = \frac{\frac{1}{Z_{\mathbb{N}}} \sum_{\underline{x} \in \mathbb{N}} \left[f(\underline{x}_i) - m_1(\underline{x})\right]^3}{m_2(\underline{x})^3}, \tag{6}$$

and the fourth standardized moment m_4,

$$m_4(\underline{x}) = \frac{\frac{1}{Z_{\mathbb{N}}} \sum_{\underline{x} \in \mathbb{N}} \left[f(\underline{x}_i) - m_1(\underline{x})\right]^4}{m_2(\underline{x})^4}, \tag{7}$$

where $\mathbb{N}$ represents the local neighborhood around $\underline{x}$, and $Z_{\mathbb{N}}$ is the number of pixels within $\mathbb{N}$.

The four statistical moments chosen to model the local tissue distribution, while simple to compute, provide important insights about the underlying tissue distribution of the local neighborhood around $\underline{x}$. The first moment about zero m_1 characterizes the central tendency of the tissue characteristics and provides a good indication of the overall type of tissue within the local neighborhood. The second central moment m_2 characterizes the spread of tissue characteristics and provides a good indication of tissue changes within the local neighborhood. The third and fourth standardized moments m_3 and m_4 characterizes the skewness and kurtosis of the tissue characteristics within a local neighborhood and allows for better discrimination between local tissue distributions, which is important since we wish to emphasize the importance of pixels with similar tissue characteristics in the superresolution process to better capture fine tissue detail in the constructed high resolution mammogram image. The local distribution models used are obtained based on 7×7 neighborhoods from the low resolution mammogram images, averaged and up-sampled to the same resolution as the high resolution mammogram image.

3.2 Constrained Optimization using Adaptive Moment-Guided Priors

Given the local tissue distribution models derived from the low resolution mammogram images $\Upsilon(\underline{x}) = \{m_1(\underline{x}), m_2(\underline{x}), m_3(\underline{x}), m_4(\underline{x})\}$, we seek to take advantage of the statistical characteristics of the underlying breast tissues being imaged to produce high resolution mammogram images with enhanced fine tissue details such that the presence of masses and microcalcifications can be

more easily identified. The mammogram image superresolution problem posed in Section 2 can be formulated as an optimization problem,

$$(\underline{\hat{g}})_{:} = \arg\min \left(\left\| \overline{\mathrm{H}}(\underline{g})_{:} - \underline{\bar{f}} \right\| \right), \tag{8}$$

where $(\underline{\hat{g}})_{:}$ is a vector representing the estimated high resolution mammogram image $\hat{g}$ in lexicographic ordering.

As stated in Section 2, the mammogram image superresolution problem is in general underdetermined, and therefore ill-posed, due to the fact that only a few acquisitions can be made in practice to limit potential harm to the patient. To obtain a unique solution to the mammogram image superresolution problem, one must impose a set of prior constraints to regularize the problem,

$$(\underline{\hat{g}})_{:} = \arg\min \left(\left\| \overline{\mathrm{H}}(\underline{g})_{:} - \underline{\bar{f}} \right\| + \left\| \Gamma(\underline{\mathrm{g}})_{:} \right\| \right), \tag{9}$$

where Γ represents the prior constraints. Given the constrained optimization problem in Eq. (9), the goal is to determine a set of prior constraints that produce a consistent, unbiased estimate of the high resolution mammogram image based on the set of low resolution mammogram images that well captures fine tissue detail in the breast region being imaged.

Using a third-order Markov model [15], a common approach to regularizing a constrained optimization problem such as that posed in Eq. (9) is to impose first-order and second-order continuity constraints on each point $\underline{x} = (x, y)$, which minimizes an approximate slope and curvature [16], respectively, and can be expressed as

$$\|\Gamma(g)\| = E_1(g) + E_2(g), \tag{10}$$

where E_1 denote the first-order constraints,

$$E_1(g) = \int\int \left[\left(\frac{\partial g}{\partial x} \right)^2 + \left(\frac{\partial g}{\partial y} \right)^2 \right] dxdy, \tag{11}$$

and E_2 denote the second-order constraints,

$$E_2(g) = \int\int \left[\left(\frac{\partial^2 g}{\partial^2 x} \right)^2 + 2\left(\frac{\partial^2 g}{\partial x \partial y} \right)^2 + \left(\frac{\partial^2 g}{\partial^2 y} \right)^2 \right] dxdy. \tag{12}$$

Based on discrete approximations of partial derivatives, the prior constraints $Q = \Gamma\Gamma^{\mathrm{T}}$ at each pixel $\underline{x}$ can be expressed in matrix form as

$$Q(\underline{x}) = \begin{bmatrix} 0 & 0 & 1 & 0 & 0 \\ 0 & 2 & -9 & 2 & 0 \\ 1 & -9 & 24 & -9 & 1 \\ 0 & 2 & -9 & 2 & 0 \\ 0 & 0 & 1 & 0 & 0 \end{bmatrix}. \tag{13}$$

where the central element of $Q(\underline{x})$ represents the pixel at $\underline{x}$.

A major limitation to using the continuity constraints defined in Eq. (13) is that it imposes stationary constraints on the entire mammogram image, regardless of the underlying tissue characteristics of the breast region being imaged. To take advantage of the tissue characteristics of the breast region being imaged to produce high resolution mammogram images with enhanced fine tissue details, we propose to adapt the prior constraints based on the local tissue statistics captured by the local tissue distribution models derived from the low resolution mammogram images $\Upsilon(\underline{x}) = \{m_1(\underline{x}), m_2(\underline{x}), m_3(\underline{x}), m_4(\underline{x})\}$. In doing so, we are imposing prior constraints in a nonstationary and nonlinear fashion such that fine tissue details are better captured in the constructed high resolution mammogram image.

Rather than using the stationary first-order and second-order constraints defined in Eq. (13), we propose to instead impose nonstationary and nonlinear prior constraints on each point $\underline{x}$ based on the likelihoods of its neighboring pixels $\{x_j \in \mathbb{N}\}$ belonging to the same tissue distribution as $\underline{x}$, which we will denote as $\mathcal{L} = \{\mathcal{L}(\underline{x}, \underline{x}_j) | x_j \in \mathbb{N}\}$. This approach is motivated by the intuition that fine tissue details and structures, such as those representing suspicious cancer-related abnormalities (e.g., masses and microcalcifications), are formed in a mammogram image by pixels with similar tissue characteristics. Therefore, adapting the level of approximation at each point in the image such that stronger constraints are imposed on pixels with strong tissue distribution similarities not only better preserves fine tissue detail, but also suppresses acquisition noise and artifacts since they have different statistical characteristics than the underlying tissue in the breast region being imaged.

Based on the aforementioned motivations, the adaptive moment-guided prior constraints Q_m at each pixel $\underline{x}$ can be expressed in matrix form as

$$Q_m(\underline{x}) = \frac{1}{K} \begin{bmatrix} 0 & 0 & \mathcal{L}_3 & 0 & 0 \\ 0 & 2\mathcal{L}_7 & -9\mathcal{L}_8 & 2\mathcal{L}_9 & 0 \\ \mathcal{L}_{11} & -9\mathcal{L}_{12} & 24\mathcal{L}_{13} & -9\mathcal{L}_{14} & \mathcal{L}_{15} \\ 0 & 2\mathcal{L}_{17} & -9\mathcal{L}_{18} & 2\mathcal{L}_{19} & 0 \\ 0 & 0 & \mathcal{L}_{23} & 0 & 0 \end{bmatrix}, \tag{14}$$

where $\mathcal{L}_i = \mathcal{L}(\underline{x}_i | \underline{x})$ represents the likelihood that $\underline{x}_i$ belongs to the same tissue distribution as $\underline{x}$, and K is a normalization term such that the sum of all constraint terms in Q_m is zero.

Since the local distribution of each pixel $\underline{x}$ is modeled using a set of statistical moments $\Upsilon(\underline{x}) = \{m_1(\underline{x}), m_2(\underline{x}), m_3(\underline{x}), m_4(\underline{x})\}$, we propose a Gibbs inter-pixel likelihood function $\mathcal{L}(\underline{x}_i | \underline{x})$ based on the weighted deviations between $\Upsilon(\underline{x}_i)$ and $\Upsilon(\underline{x})$,

$$L(\underline{x}_i | \underline{x}) = \prod_{j=1}^{4} \exp\left(-\alpha_j \left(m_j(\underline{x}_i) - m_j(\underline{x}) \right)^2 \right), \tag{15}$$

where $\alpha_j = 0.25$ is the weight assigned to the statistical moment m_j. Based on Eq. (15), the greater the deviation in statistical moments between $\Upsilon(\underline{x}_i)$ and $\Upsilon(\underline{x})$, the lower the likelihood of $\underline{x}_i$ belonging to the same distribution as $\underline{x}$. Therefore, the likelihood functions $\mathcal{L}(\underline{x}_i|\underline{x})$ in Eq. (14) act as weighting factors that emphasize pixels with similar local tissue distributions in the prior constraints.

What the proposed nonstationary moment-guided prior constraints described in Eq. (14) allow for is adaptive per-pixel refinement of information contribution from the low resolution mammogram images to the generation of the high resolution mammogram image, where fine tissue detail formed by pixels with similar breast tissue characteristics are emphasized for improved visualization of suspicious abnormalities such as masses and microcalcifications.

Given the nonstationary moment-guided prior constraints described in Eq. (14), the solution of the constrained optimization problem can be defined based on the Tikonov regularization equation [21],

$$(\hat{\underline{g}})_{:} = \left(\overline{\mathrm{H}}^T\overline{\mathrm{H}} + Q_m\right)^{-1}\mathrm{H}^T\underline{\bar{f}}. \tag{16}$$

Eq. (16) can be rearranged in the form of $A(\hat{\underline{g}})_{:} = \underline{b}$, where $A = \left(\overline{\mathrm{H}}^T\overline{\mathrm{H}} + Q_m\right)^{-1}$ and $\underline{b} = \mathrm{H}^T\underline{\bar{f}}$. The high resolution mammogram image $(\hat{\underline{g}})_{:}$ is constructed by computing the estimated solution to the constrained optimization problem (Eq. (16)) based on the moment-guided priors using an efficient conjugate gradient approach [19].

4 Experimental Results

The proposed SMA superresolution method was performed using real mammogram images obtained from the Mammographic Image Analysis Society (MIAS) database [20] to investigate its effectiveness at enhancing tissue detail for better visualization. The dedicated mammography machine used to acquire the mammogram images was a Joyce-Loebl microdensitometer SCANDIG-3, with a linear response in the optical density range $0-3.2$. Each set of tested mammogram images consists of six 8-bit grayscale images with a pixel resolution of $200\mu m \times 200\mu m$ and a 25μm shift interval. The tested data-sets can be described as follows:

1. **M1**: MIA database mammogram 001, Background tissue: fatty-glandular, Class of abnormality: well-defined/circumscribed masses, Severity of abnormality: benign.

2. **M2**: MIA database mammogram 015, Background tissue: fatty-glandular, Class of abnormality: well-defined/circumscribed masses, Severity of abnormality: benign.

3. **M3**: MIA database mammogram 181, Background tissue: fatty-glandular, Class of abnormality: spiculated masses, Severity of abnormality: malignant.

4. **M4**: MIA database mammogram 206, Background tissue: fatty, Class of abnormality: spiculated masses, Severity of abnormality: malignant.

5. **M5**: MIA database mammogram 209, Background tissue: fatty-glandular, Class of abnormality: calcification, Severity of abnormality: malignant.

6. **M6**: MIA database mammogram 211, Background tissue: fatty-glandular, Class of abnormality: calcification, Severity of abnormality: malignant.

To test the effectiveness of the SMA method, the low resolution mammogram images in each tested data-set were combined using the SMA method to produce a high resolution mammogram image with a pixel resolution of $50\mu m \times 50\mu m$. Bicubic interpolation and the method proposed by Kennedy et al. [10]. To empirically evaluate the effectiveness of the proposed method at high resolution mammogram image reconstruction, the Peak-Signal-to-Noise Ratio (PSNR) was calculated between the generated high resolution image and the corresponding reference image for each of the tested methods.

The PSNR results for all tested data-sets are shown in Table 1. The SMA method noticeably outperform the other tested methods in terms of PSNR for all tested data-sets. This improvement in PSNR demonstrates the SMA method's ability to generate accurate high resolution mammogram image reconstructions compared to existing approaches.

For visual comparisons, regions of interests were extracted from the breast region in the reconstructed high resolution mammogram images for each of the tested data-sets (Figs. 1-4). Contrast enhancement using intensity normalization was performed on the mammogram images shown to improve the visibility of tissue details in the figures provided. On visual inspection, the high resolution mammogram images generated using the SMA method provides noticeably better visibility of fine tissue detail when compared to the other tested methods.

In Fig. 1, the shape and boundaries of the circumscribed and spiculated masses are noticeably better defined in the high resolution mammogram images generated using the SMA method when compared to the other tested methods. In Fig. 2, the nodule boundaries are poorly defined in the high resolution mammogram images generated using bicubic interpolation and the Kennedy method. On the other hand, the nodule boundaries are clearly defined with high structural contrast in the high resolution mammogram image generated using the SMA method, which is important for visualizations during the clinical screening process.

In Figs. 3-4, there are calcifications embedded behind dense tissues, which are very difficult, even impossible in the case of Fig. 3, to identify in the high resolution mammogram image generated using bicubic interpolation. The Kennedy method generates high resolution mammogram images that provide noticeably better calcification definition than bicubic interpolation, but the overall shape and boundaries of the calcifications remain difficult to interpret. In both cases, the SMA method generated high resolution mammogram images with noticeably better calcification shape and boundary definition when compared to the other tested methods, making it easier to identify and interpret the calcifications embedded between the dense tissues during the clinical screening process. These tests show that the SMA method is capable of generating high resolution mammogram images with improved fine tissue detail definition that allows for greater visibility of suspicious abnormalities in the breast region such as masses and microcalcifications.

Table 1. PSNR for Tested Data-sets

Data-set	PSNR (dB)		
	Bicubic Interpolation	[10]	SMA Method
M1	39.0111	45.2684	48.6317
M2	38.2615	44.0657	47.2658
M3	36.8680	42.8792	46.9089
M4	37.6002	42.9916	46.7166
M5	37.4122	43.5773	47.4197
M6	37.8646	43.6795	47.3050

5 Conclusions

In this paper, a novel superresolution method designed to enhance mammogram images for clinical mammogram screening is proposed. Based on local tissue distributions modeled using statistical moments, the proposed method adapts to the underlying tissue characteristics of the breast region being imaged to better capture fine tissue detail, thus enhancing the visibility of suspicious cancer-related abnormalities such as masses and microcalcifications. Experimental results using real mammographic images show that the proposed SMA method is capable of achieving improved tissue detail preservation when compared to existing methods. Future work include integrating additional adaptive prior constraints into the SMA method to simultaneously enhance tissue detail and correct for signal nonuniformities in the acquired mammogram images, as well as investigate the effectiveness of the SMA method for enhancing medical images acquired using different imaging technologies, such as MR and ultrasound imagery.

Acknowledgment

This research has been sponsored in part by the Natural Sciences and Engineering Research Council of Canada. The authors would like to thank the Mammographic Image Analysis Society for the mammographic images used during testing.

References

[1] P. Boyle and B. Levin, "Breast Cancer," *World Cancer Report 2008*, IARC Press, pp. 412–417, 2008.

[2] World Health Organization, "Fact sheet No. 297: Cancer," `http://www.who.int/mediacentre/factsheets/fs297/en/index.html`, Retrieved Oct. 4, 2009.

[3] American Cancer Society, "Breast Cancer Facts & Figures 2009-2010," `http://www.cancer.org/downloads/STT/F861009_final209-08-09.pdf`, Retrieved Oct. 4, 2009.

[4] P. Boyle and B. Levin, "Screening for Breast Cancer," *World Cancer Report 2008*, IARC Press, pp. 296–301, 2008.

[5] D. Robinson, S. Farsiu, J. Lo, P. Milanfar, and C. Toth, "Efficient Multiframe Registration of Aliased X-Ray Images", *Proc. 41th Asilomar Conference on Signals, Systems, and Computers*, 2007.

[6] T. Aoki, Y. Ishida, H. Morii, Y. Tomita, G. Ohashi, J. Temmyo, and Y. Hatanaka, "Superresolution X-ray imaging by CdTe discrete detector arrays," *Proceedings of SPIE - Hard X-Ray and Gamma-Ray Detector Physics VII*, vol. 5922, 2005.

[7] R. Peeters, P. Kornprobst, M. Nikolova, S. Sunaert, T. Vieville, G. Malandain, R. Deriche, O. Faugeras, M. Ng, P. Van Hecke, "The use of super-resolution techniques to reduce slice thickness in functional MRI," *Int. J. Imag. Sys. and Technology*, vol. 14, no. 3, pp. 131–138, 2004.

[8] S. Peled and Y. Yeshurun, "Superresolution in MRI: Application to Human White Matter Fiber

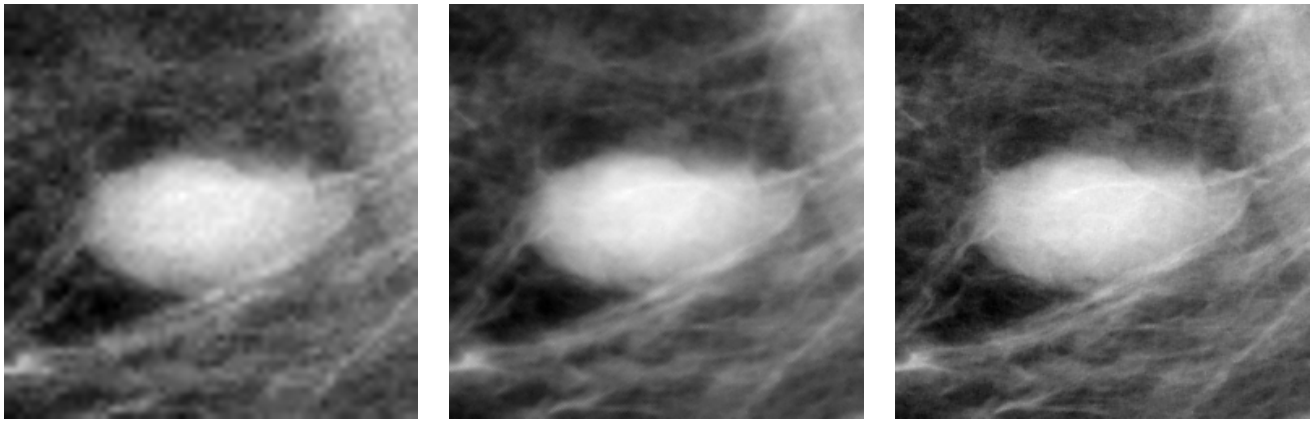

Figure 1. A region-of-interest from M3 (from left to right): a) bicubic interpolation, b) Kennedy method [10], c) SMA method

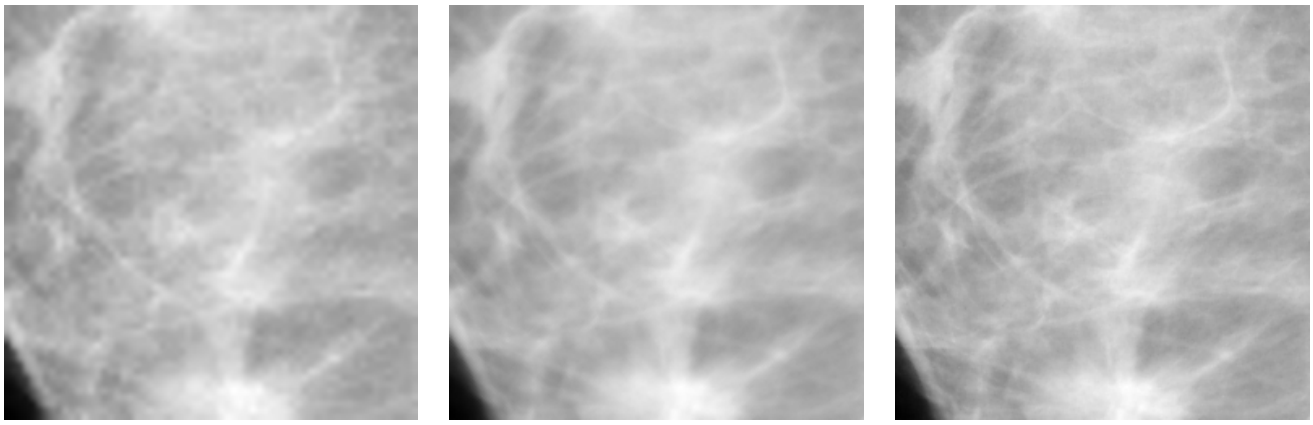

Figure 2. A region-of-interest from M4 (from left to right): a) bicubic interpolation, b) Kennedy method [10], c) SMA method

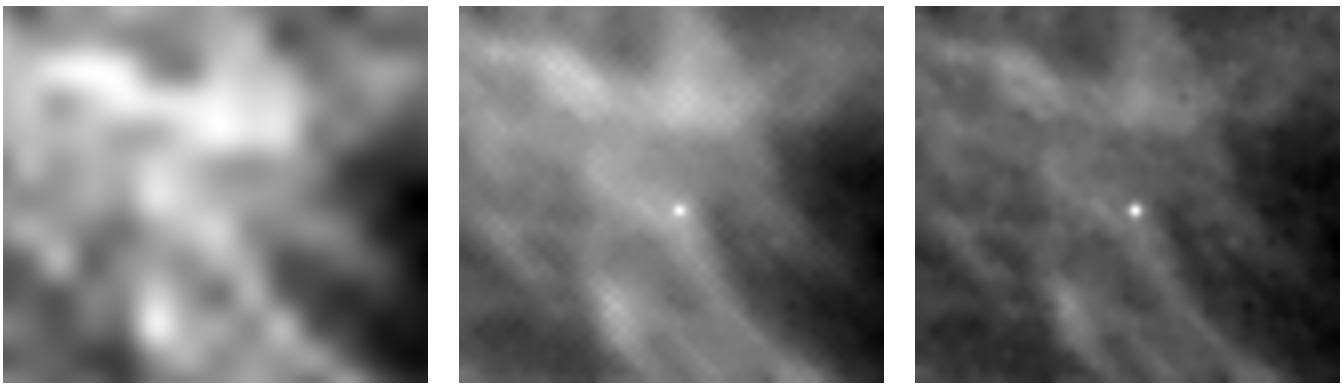

Figure 3. A 4x zoomed-in region-of-interest from M4 (from left to right): a) bicubic interpolation, b) Kennedy method [10], c) SMA method

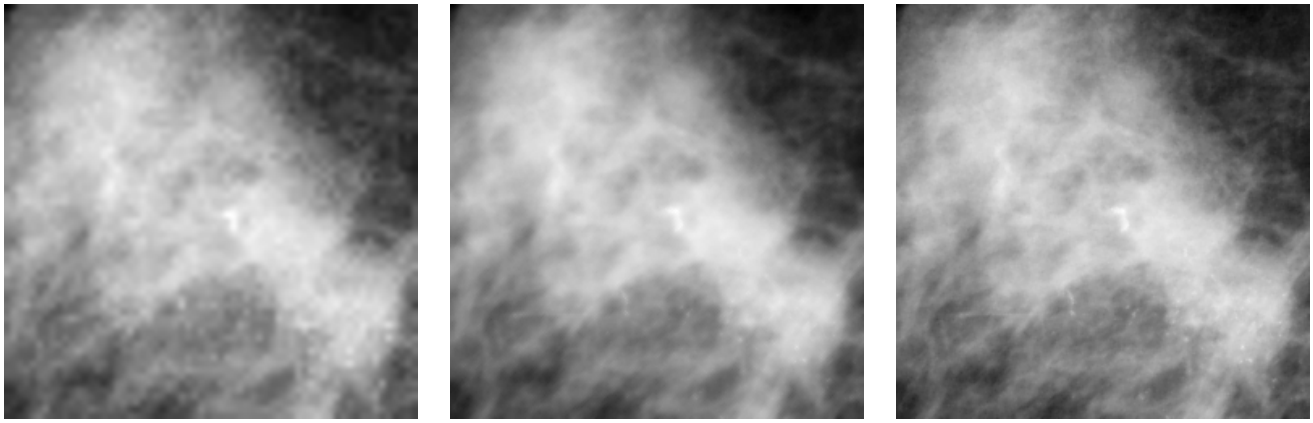

Figure 4. A region-of-interest from M5 (from left to right): a) bicubic interpolation, b) Kennedy method [10], c) SMA method

Tract Visualization by Diffusion Tensor Imaging," *Magn. Reson. Med. J.*, vol. 45, no. 1, pp. 29-35, 2001.

[9] H. Greenspan, G. Oz, N. Kiryati, and S. Peled, "Super-resolution in MRI," *Proc. IEEE Int. Symp. Biomedical Imaging*, pp. 943-946, 2002.

[10] J. Kennedy, O. Israel, A. Frenkel, R. Bar-Shalom, and H. Azhari, "Super-resolution in PET imaging," *IEEE Trans. on Medical Imaging*, vol. 25, no. 2, pp. 137-147, 2006.

[11] J. Kennedy, O. Israel, A. Frenkel, R. Bar-Shalom, and H. Azhari, "Improved Image Fusion in PET/CT Using Hybrid Image Reconstruction and Super-Resolution," *International Journal of Biomedical Imaging*, vol. 2007, Article ID 46846, 10 pages, 2007.

[12] M. Irani and S. Peleg, "Improving resolution by image registration," *Proceedings of CVGIP: Graphical Models and Image Processing*, vol. 53, no. 3, pp. 231-239, 1991.

[13] J. Hsu, C. Yen, C. Li, M. Sun, B. Tian, and M. Kaygusuz, "Application of wavelet-based POCS super-resolution for cardiovascular MRI image enhancement," *Proc. International Conference on Image and Graphics*, pp. 572-575, 2004.

[14] K. Sauer and J. Allebach, "Iterative reconstruction of band-limited images from nonuniformly spaced samples," *IEEE Transactions on Circuits and Systems*, vol. 34, no. 12, pp. 1497-1506, 1987.

[15] A. Rangarajan and R. Chellappa, "Markov random field models in image processing," *Handbook of Brain theory and Neural Networks*, MIT Press, Cambridge, MA, pp. 564-567, 1998.

[16] G. Wahba, Spline models for observational data. Philadelphia: Society for Industrial and Applied Mathematics, 1990.

[17] C. Paige and M. Saunders, "LSQR: an algorithm for sparse linear equations and sparse least squares," *ACM Transactions On Mathematical Software*, vol. 8, no. 1, pp. 43-71, 1982.

[18] G. Barnes and D. Chakraborty, "Radiographic mottle and patient exposure in mammography", *Radiology*, vol. 145, pp. 815-821, 1982.

[19] R. Salakhutdinov and S. Roweis, "Adaptive Overrelaxed Bound Optimization Methods," *Proceedings of the International Conference on Machine Learning,* vol. 20, pp. 664-671, 2003.

[20] J. Suckling, J. Parker, D. Dance, S. Astley, I. Hutt, C. Boggis. I. Ricketts, E. Stamatakis, N. Cerneaz, S. Kok, P. Taylor, D. Betal and J. Savage, "The mammographic images analysis society digital mammogram database," *Exerpta Medica. International Congress Series,* vol. 1069, pp. 375-378, 1994.

[21] A. Tikhonov, "On the stability of inverse problems," *Dokl. Akad. Nauk SSSR,* vol. 39, no. 5, pp. 195-198, 1943.